Icarus 321 (2019) 564–571

Contents lists available at ScienceDirect

Icarus

journal homepage: www.elsevier.com/locate/icarus

# Measuring the Yarkovsky effect with Las Cumbres Observatory

Sarah Greenstreet[*,a,b,c,d], Davide Farnocchia[e], Tim Lister[c]

[a] B612 Asteroid Institute, 20 Sunnyside Ave, Suite 427, Mill Valley, CA 94941, USA
[b] DIRAC Center, Department of Astronomy, University of Washington, 3910 15th Ave NE, Seattle, WA 98195, USA
[c] Las Cumbres Observatory, 6740 Cortona Drive, Suite 102, Goleta, CA 93117, USA
[d] University of California, Santa Barbara, Santa Barbara, CA 93106, USA
[e] Jet Propulsion Laboratory, California Institute of Technology, 4800 Oak Grove Drive, Pasadena, CA 91109, USA

ARTICLE INFO

*Keywords:*
Minor planets
Asteroids: general — telescopes — astrometry

ABSTRACT

The Las Cumbres Observatory (LCOGT) provides an ideal platform for follow-up and characterization of Solar System objects (e.g. asteroids, Kuiper belt objects (KBOs), comets, and near-Earth objects (NEOs)) as well as for the discovery of new objects. The LCOGT network allows for regular monitoring of a sample of targets, such as that of NEOs for which we can attempt to measure the Yarkovsky effect. We have used LCOGT's global network of nine 1.0-m telescopes to measure the Yarkovsky effect on 36 asteroids through precise astrometric measurements using the Gaia-DR1 catalog; 18 (50%) of the 36 asteroids yielded $> 3\sigma$ Yarkovsky detections. The target asteroids were selected through simulated observations each month to determine the objects for which new astrometry would yield the highest likelihood of a Yarkovsky detection. The Gaia-DR1 release has greatly improved the quality of the astrometry obtained, making the detection of the Yarkovsky effect more likely and secure by greatly reducing systematic catalog zonal errors. LCOGT is ideally suited to perform these observations due to its ability to monitor many targets over several days by employing dynamic scheduling, weather avoidance, and use of multiple sites around the globe.

## 1. Introduction

### 1.1. Las Cumbres Observatory

Las Cumbres Observatory (LCOGT) [1] is a not-for-profit observatory for studying time-domain astronomy. LCOGT has built and is operating a global network of two 2.0-m, nine 1.0-m, and ten 0.4-m robotic telescopes as an integrated telescope network (Brown et al., 2013; Boroson et al., 2014; Volgenau and Boroson, 2016). The two 2.0-m telescopes (the Faulkes North and Faulkes South telescopes) are located in Hawaii and Australia. The nine 1.0-m telescopes are largely located in the southern hemisphere in Chile, South Africa, Australia, and Texas; LCOGT has recently received two grants to add three more 1.0-m telescopes to the network in the northern hemisphere in Texas (one) and the Canary Islands (two). The ten 0.4-m telescopes are located at each of the 2.0-m and 1.0-m telescope locations with the addition of the Canary Islands.

This versatile network has been designed for both rapid response to target of opportunity and transient events as well as monitoring long-term, slowly-changing astronomical phenomena. The network's global coverage and available telescope apertures make it excellent for the characterization of Solar System objects, including detecting the Yarkovsky effect through astrometric measurements of asteroids.

Unlike classically scheduled telescopes with either attended or remote manual observing, observing requests on the LCOGT network are submitted through the observing portal website[2] or programmatically through an API. These observing requests contain the target, the type of telescope desired, details of the exposures and filters required, and any timing constraints. The requests from all programs are examined by the LCOGT scheduler[3] (Saunders et al., 2014), which dynamically considers the request constraints and the state of the telescope network before assigning each request a score; those that have the best scores are scheduled across the network as a whole. The LCOGT scheduler reexamines all requests every 20 min and adjusts the scheduled requests as necessary.

Observation data from the instruments and telescopes are

* Corresponding author at: B612 Asteroid Institute, 20 Sunnyside Ave, Suite 427, Mill Valley, CA 94941, USA.
*E-mail address:* sarah@b612foundation.org (S. Greenstreet).
[1] https://lco.global/.
[2] https://observe.lco.global/.
[3] https://schedule.lco.global/.

https://doi.org/10.1016/j.icarus.2018.11.032
Received 3 August 2018; Received in revised form 27 November 2018; Accepted 29 November 2018
Available online 04 December 2018
0019-1035/ 

transferred back to LCOGT headquarters and processed in near real-time as well as reprocessed at the end of the night and distributed through an online science archive[4]. For more information on LCOGT data processing, see Section 2.3.

These facilities were used to build the LCOGT Follow-up Network (Lister et al., 2015) and NEOexchange[5], which allow the ingest, planning, scheduling, and data analysis for moving Solar System targets of all kinds on the LCOGT network. NEOexchange allows for the creation and maintenance of a list of targets for multiple observational programs, including the one described below for Yarkovsky targets, and handles planning and scheduling of these targets at optimum times on the LCOGT telescope network.

### 1.2. The Yarkovsky effect

The Yarkovsky effect is a force that acts on rotating asteroids as they anisotropically radiate heat absorbed by the Sun, causing small secular changes in their semimajor axes over time (Vokrouhlický et al., 2015a). The diurnal Yarkovsky effect is caused by the lag between the time it takes for an asteroid to absorb incident solar radiation and re-emit the energy as heat as well as the difference in direction between the absorption and re-emission of radiation as the asteroid rotates. If the asteroid is a prograde rotator (i.e., it rotates in the same direction as its orbital motion), as the heated side of the asteroid rotates away from pointing at the Sun, the net force on the asteroid is in its direction of motion, causing the asteroid's semimajor axis to slowly increase and the asteroid to drift outward from the Sun. If the asteroid is in retrograde rotation, the net force is opposite the direction of motion, and the asteroid's semimajor axis will be slowly decreased, drifting it inward toward the Sun. The small drift in semimajor axis due to the Yarkovsky effect scales as $1/D$ (where $D$ is the diameter of the asteroid) and so is most important for smaller asteroids; the Yarkovsky effect is harder to detect for larger asteroids due to this dependence. For example, (101955) Bennu ($D \approx 0.5$ km) has a mean semimajor axis drift rate of $da/dt = -284$ m/yr (Chesley et al., 2014), which means that in 10 years, the semimajor axis changes by 3 km = 2e-8 AU due to the Yarkovsky effect. In order to detect such a drift, the semimajor axis needs to be known to this level of accuracy. For an object 10 times larger, the semimajor axis needs to be known to the level of 2e-9 AU, making the Yarkovsky effect harder to detect for larger and larger objects. The acceleration accumulates quadratically in the mean anomaly with the time span of the dataset and can be detected from fits to astrometric measurements for well-constrained orbits (Farnocchia et al., 2013b).

In addition, the Yarkovsky acceleration decreases with distance from the Sun and so is smaller for a main-belt asteroid than for a near-Earth object (NEO) of the same size. A closer proximity to an asteroid also provides more powerful angular measurements and ability to obtain radar observations, which can greatly aid in measuring the Yarkovsky effect. Close approaches can magnify the offset caused by the Yarkovsky effect thus making it easier to detect. For these reasons, most Yarkovsky detections are made for NEOs and not main-belt asteroids.

### 1.3. Applications of the Yarkovsky effect

One of the most important applications of the Yarkovsky effect is in determining impact probabilities, which can be modified when the Yarkovsky effect is considered (Giorgini et al., 2002; 2008; Farnocchia et al., 2013a; Farnocchia and Chesley, 2014; Chesley et al., 2014; Spoto et al., 2014; Vokrouhlický et al., 2015b). For long-term impact predictions or when scattering planetary encounters perturb the orbit, even a small drift in semimajor axis can make the difference between a near-miss and an impact for asteroids that pass close to the Earth.

The Yarkovsky effect has also helped to explain the transfer of asteroids and meteoroids from the main-belt to near-Earth space as well as the structure of asteroid families (Bottke et al., 2006). Main-belt resonances are partially replenished by Yarkovsky-driven semimajor axis drift of asteroids near the resonance boundaries that can move those asteroids into the resonance; eccentricity-pumping mechanisms within the resonance then push the asteroids into near-Earth space (pericenter $q < 1.3$ AU).

Measurements of the Yarkovsky effect can yield constraints on asteroid physical parameters such as obliquity, rotation rate, surface thermal inertia, bulk density, and mass (Bottke et al., 2006). Though disentangling these quantities is not possible with Yarkovsky alone, constraints can be made without the need for spacecraft flybys or binary asteroids. In addition, observations in the thermal infrared with facilities like the James Webb Space Telescope (JWST) can help constrain thermal inertia surface properties, which could additionally help constrain the Yarkovsky effect for individual asteroids and vice versa. These physical properties are important for spacecraft sample return missions targeting asteroids, such as the OSIRIS-REx mission launched in September 2016 to the asteroid (101955) Bennu. The measured semimajor axis drift rate of $da/dt = -284$ m/yr, together with Spitzer and radar observations, allowed Chesley et al. (2014) to estimate the density and mass of Bennu. Spacecraft safety, trajectory, and sampling and the success of completing science goals depend on precisely known orbital parameters and physical properties of the asteroid.

### 1.4. Past Yarkovsky measurements

The Yarkovsky effect is difficult to predict; the magnitude depends on generally unknown asteroid physical properties. The Yarkovsky effect has been adequately measured for $< 100$ asteroids as of October 2016 when our observing campaign began (Chesley et al., 2015), including (6489) Golevka ($D \approx 0.5$ km), measured to drift $\approx 15$ km over a 12-year period (Chesley et al., 2003), (101955) Bennu ($D \approx 0.5$ km), (mean semimajor axis drift rate $da/dt = -284$ m/yr (Chesley et al., 2014)), a few tens of detections by Nugent et al. (2012) (one of which overlaps with our targets and agrees with our results) and Farnocchia et al. (2013b), (three of which overlap with our targets and agree with our results) and a number of other asteroids (e.g., Vokrouhlický et al. (2008); Farnocchia et al. (2014); Mommert et al. (2014)). 10 of our 46 targets also appear in Greenberg et al. (2017), 9 of them for which we get a $> 3\sigma$ Yarkovsky detection; all but four of these overlapping targets agree within the error bars, but none are fractionally different by $> 35\%$.[6] In addition, there are hundreds of candidate Yarkovsky drifters (Nugent et al., 2012).

## 2. Methods

A small number of high quality, timely astrometric measurements can reveal deviations from a gravity-only trajectory, making the Yarkovsky signal detectable (Binzel, 2003). We used LCOGT's global network of nine 1.0-m telescopes, which act as a single observatory (Brown et al., 2013; Boroson et al., 2014; Volgenau and Boroson, 2016), to make astrometric measurements of candidate Yarkovsky drifters; the observations were dynamically scheduled across the network (see Section 1.1 for more information on the LCOGT scheduler).

[4] https://archive.lco.global/.

[5] https://lco.global/neoexchange/.

[6] Shortly after our paper was submitted for publication, a paper by Del Vigna et al. (2018) was published online with Yarkovsky detections of 87 near-Earth asteroids. The Del Vigna et al. (2018) paper made use of our publicly available astrometry and their independent results are consistent with the ones presented in this paper.

### 2.1. Target selection

Targets for this program were drawn from the full NEO catalog, where we selected a small number of targets that were predicted to best yield a Yarkovsky measurement in a given month. On a monthly basis, we searched the entire NEO catalog to identify the objects that could be observable to LCOGT telescopes by requiring that they were brighter than $V = 21.5$ and had a solar elongation greater than 60°. The vast majority of the targets were visible from the southern hemisphere where all but one of LCOGT's 1.0-m telescopes are currently located (see Section 1.1 for telescope locations).

Among the selected objects, we identified the ones for which LCOGT observations would be beneficial in constraining the Yarkovsky effect. To this purpose, we added to the force model a transverse acceleration $A_2/r^2$, where $r$ is the heliocentric distance in AU and $A_2$ is a free parameter to be estimated from the fit. The parameter $A_2$ relates to the Yarkovsky driven semimajor drift by:

$$\frac{da}{dt} = \frac{2A_2}{na(1-e^2)} \tag{1}$$

where $a$ is the semimajor axis in AU, $e$ the eccentricity, and $n$ is the orbital mean motion (Farnocchia et al., 2013b). We estimated the current uncertainty in $A_2$ from the current orbit fit as well as that we would have by adding simulated data when the object was observable to the LCOGT telescopes. Then, we selected only the objects for which the uncertainty in $A_2$ decreased by a factor of two or more when adding simulated LCOGT astrometry.

The final selection filter was based on an assessment of the likelihood of actually detecting a Yarkovsky drift thanks to LCOGT observations. Based on the absolute magnitude $H$ of each object, we inferred the diameter $D$ assuming an albedo of 0.154. Since $A_2$ is inversely proportional to the diameter (Farnocchia et al., 2013b), we computed an extrapolated value for $A_2$ by scaling from that of Bennu (Chesley et al., 2014; Farnocchia et al., 2013b):

$$(A_2)_{extrapolated} = |(A_2)_{Bennu}|\frac{D_{Bennu}}{D} \tag{2}$$

We selected the objects for which $(A_2)_{extrapolated}$ was larger than three times the $A_2$ uncertainty computed by adding simulated LCOGT data. In total, 46 targets were found during the observing program from November 2016 to May 2018. Table 1 gives the list of selected Yarkovsky targets and their observability windows for the LCOGT observing program.

While these conditions allowed us to identify the objects with the highest chance of yielding a Yarkovsky detection, there was no guarantee that additional observations would lead to a detection of the Yarkovsky effect. In fact, the actual value of $A_2$ can be smaller in magnitude than $(A_2)_{extrapolated}$ depending on the physical properties of the observed object, e.g., a mid-range obliquity or a large bulk density, since Bennu has several parameters that maximize its semimajor axis drift rate such as an extreme obliquity (175°) and a low density ($1260 \pm 70$ kg/m$^3$) (Chesley et al., 2014); the semimajor axis drift rate scales as

$$\frac{da}{dt} \propto \frac{cos(\gamma)}{\rho D} \tag{3}$$

where γ is the obliquity of the asteroid equator with respect to its orbital plane, ρ is the bulk density of the asteroid, and $D$ is the asteroid diameter (Chesley et al., 2014). Chesley et al. (2015) referred to this category of low-SNR Yarkovsky estimates as "weak detections".

### 2.2. Observations

The observing program covered a period of 19 months from November 2016 to May 2018. Observations were performed using the nine 1.0-m telescopes and Sinistro optical imagers of the LCOGT Network. The cameras utilize a Fairchild 4096 × 4096 CCD with 15 $\mu m$ pixels, giving a pixel scale of 0.389″/pixel in bin 1 × 1 and a field of view of 26.7′ × 26.7′. The small pixel size allows better sampling of the seeing PSF (typically $\approx 1.3'' - 2.5''$) and good astrometric accuracy. In addition, the large field of view allows a greater number of astrometric reference stars to be used, resulting in a better determined astrometric solution. Observations were carried out in PanSTARRS-$w$ (equivalent to SDSS-$g' + r' + i'$; Tonry et al., 2012). The observations used the maximum exposure time allowed by the object's rate of motion at the predicted time of observation that would not result in trailing. Calculation of the observability, brightness, and rate of motion of each target and the submittal of the observations to the LCOGT robotic telescope network were performed using the routines of LCOGT's web-based minor planet follow-up portal, NEOexchange[7] (Lister et al., 2015).

Each observation visit for an object consisted of 20–30 min blocks containing a number of observations that would fill the block given the exposure time needed to avoid trailing losses. These visits were repeated at an approximately 2-h cadence across the global telescope network for typically 2–3 days around the time of best observability for a candidate. This spacing allowed for extra insurance in the case of bad weather, the target being obscured by bright stars, or competition on the network. The majority of targets were observed during the three weeks of the month centered around new Moon. This sort of low intensity observational program over a prolonged period is ideal for a robotic telescope network such as that of LCOGT.

### 2.3. Data reduction

Data taken on the telescopes of the LCOGT network is automatically transferred back to the headquarters in Santa Barbara, CA and pipeline processed. This occurs in near-real time (so called "quicklook" processing, typically within ≈ 10–15 minutes of shutter close) and again at the end of the night at the particular observing site. This 'end of night' processing makes use of any new bias, dark, or flat field frames that were obtained during that night.

The data reduction is carried out using the BANZAI pipeline (McCully et al., 2018), which follows the standard steps of assembling master calibration frames from the individual bias, dark, and flat field frames and then applying these to the science images to perform bad pixel masking, bias subtraction, dark current correction, and flat field division. Crosstalk correction and gain normalization between the individual quadrants and amplifiers of the Sinistro cameras' Fairchild CCD is also performed. An astrometric solution is performed using the *astrometry.net* software (Lang et al., 2010), which makes use of the 2MASS catalog (Skrutskie et al., 2006) as input. A catalog of sources detected in the frame (having a certain minimum number of pixels more than 10$\sigma$ above the fitted sky background) is also produced using SEXTRACTOR (Bertin and Arnouts, 1996). Finally the reduced frames, source catalog, and associated master calibration frames are uploaded to the LCOGT science archive[8] for distribution to end-users and from which we obtained the data for further astrometric analysis.

As detailed below in Section 2.4, we did not make use of this pipeline-produced astrometric solution and source catalog, but instead redetermined a new astrometric solution using Gaia-DR1 (Gaia Collaboration et al., 2016) and photometric solution for the per-frame zeropoint using the ASTROMETRICA software[9]. This involved use of a third order polynomial in the $x$, $y$ coordinates of the CCD frame and iterative outlier rejection in both position and magnitude of the cross-matched stars obtained from the Gaia-DR1 catalog. The formula for the transformation from the measured coordinates on the CCD ($x'$, $y'$) to the

[7] https://lco.global/neoexchange/.
[8] https://archive.lco.global/.
[9] https://www.astrometrica.at/.

**Table 1**
List of target Yarkovsky candidates. Radar indicates those candidates for which radar observations are available. The observability window is the time during the observing program the target was visible to LCOGT telescopes. The V mag range is for the observability window. Those targets observed with zero telescopes were attempted but not observed due to weather or competition on the network.

| Yarkovsky Candidate | Radar | Observability Window | H mag | V mag | # Telescopes Used |
|---|---|---|---|---|---|
| (480820) 1998 VF32 | | Nov 2016 | 21.1 | 20.4–21.1 | 0 |
| (480808) 1994 XL1 | | Nov – Dec 2016 | 20.9 | 18.5–21.4 | 4 |
| (481442) 2006 WO3 | | Nov – Dec 2016 | 21.6 | 18.3–21.3 | 6 |
| (480883) 2001 YE4 | x | Nov – Dec 2016 | 20.7 | 17.0–19.7 | 1 |
| (348306) 2005 AY28 | x | Dec 2016 | 21.5 | 20.6–22.5 | 3 |
| (163023) 2001 XU1 | | Dec 2016 | 19.3 | 18.4–18.9 | 1 |
| 2012 YK | | Dec 2016 | 23.0 | 18.8–21.6 | 3 |
| (226514) 2003 UX34 | x | Dec 2016 | 20.1 | 16.5–20.1 | 0 |
| 1995 CR | | Dec 2016 | 21.7 | 20.1–21.5 | 0 |
| (192559) 1998 VO | | Jan 2017 | 20.3 | 20.8–21.7 | 9 |
| (265482) 2005 EE | x | Jan 2017 | 21.2 | 17.9–18.3 | 7 |
| 2001 SQ263 | | Jan 2017 | 22.4 | 21.7–22.1 | 0 |
| 2011 EP51 | | Jan – Feb 2017 | 25.2 | 20.8–23.5 | 9 |
| (364136) 2006 CJ | x | Feb 2017 | 20.2 | 18.4–20.4 | 4 |
| (494710) 2005 MO13 | | May – Jun 2017 | 20.8 | 19.2–20.5 | 1 |
| (495829) 1995 LG | | May – Jun 2017 | 18.7 | 19.2–21.7 | 2 |
| (154590) 2003 MA3 | | May – Jun 2017 | 21.7 | 21.4–22.9 | 2 |
| 2011 KE3 | | Jun 2017 | 23.9 | 21.6–22.2 | 1 |
| (437841) 1998 HD14 | | Jun 2017 | 21.0 | 20.1–20.3 | 2 |
| (326354) 2000 SJ344 | | Jun 2017 | 22.7 | 21.1–21.7 | 1 |
| 2003 DZ15 | x | Jun 2017 | 22.3 | 21.7–23.0 | 1 |
| 2000 HB24 | | Jun 2017 | 23.7 | 20.4–21.7 | 0 |
| (162183) 1999 NB5 | | Jun – Jul 2017 | 21.1 | 21.6–22.5 | 2 |
| (496901) 2001 HB | | Jul 2017 | 20.4 | 21.3–21.5 | 2 |
| (499998) 2011 PT | | Jul – Sep 2017 | 23.9 | 20.3–21.9 | 2 |
| 2006 TU7 | | Sep 2017 | 21.9 | 19.9–22.0 | 3 |
| 2012 TC4 | x | Oct 2017 | 26.7 | 16.0–20.8 | 0 |
| (503941) 2003 UV11 | x | Oct 2017 | 19.5 | 14.4–19.7 | 4 |
| 2007 TF68 | | Oct 2017 | 22.7 | 19.9–21.0 | 4 |
| (513312) 2007 DM41 | | Oct 2017 | 22.0 | 18.9–20.4 | 2 |
| (376879) 2001 WW1 | | Oct 2017 | 22.2 | 21.4–22.4 | 3 |
| (497113) 2004 EK1 | | Nov 2017 | 22.2 | 21.0–21.7 | 2 |
| (506590) 2005 XB1 | | Nov 2017 | 22.0 | 19.4–22.1 | 2 |
| (506491) 2003 UW29 | | Nov 2017 | 20.6 | 21.5–21.8 | 2 |
| (3361) 1982 HR | | Nov 2017 | 19.03 | 15.3–16.9 | 2 |
| (234145) 2000 EW70 | x | Nov 2017 | 21.3 | 18.8–20.0 | 3 |
| (216985) 2000 QK130 | | Jan 2018 | 21.0 | 19.7–20.6 | 3 |
| 2006 AL4 | | Jan 2018 | 24.9 | 19.5–21.0 | 0 |
| (388189) 2006 DS14 | | Jan – Feb 2018 | 20.5 | 18.8–21.4 | 4 |
| 2016 CO246 | | Feb 2018 | 25.9 | 20.6–21.9 | 0 |
| (267940) 2004 EM20 | | Mar 2018 | 20.3 | 17.5–19.2 | 3 |
| (516435) 2004 FJ29 | | Mar 2018 | 21.3 | 19.9–21.8 | 3 |
| 2003 FY6 | | Mar – Apr 2018 | 22.4 | 18.5–21.3 | 1 |
| 2010 JO33 | | Apr 2018 | 25.0 | 20.7–22.0 | 3 |
| 2010 GD35 | | Apr 2018 | 24.6 | 19.6–23.3 | 0 |
| 2004 RQ252 | | May 2018 | 22.4 | 21.4–21.6 | 0 |

standard co-ordinates in the tangent plane ($X$, $Y$) are given by standard cubic polynomials.

Following the astrometric and photometric solution of the frames, the target asteroid's position and brightness were measured by centroiding on the object in each of the frames. The resulting right ascension (RA), declination (Dec), and magnitude measurements in MPC1992 format[10] were combined with the existing information for the object from the MPC database and a perturbed orbit (using the planets Mercury–Neptune plus the Moon as perturbers) was fitted to the combined observations using FIND_ORB[11].

### 2.4. Using Gaia for astrometric reduction

As discussed above, we made use of the Gaia-DR1 catalog (Gaia Collaboration et al., 2016) to perform the astrometric reduction. The release of the first Gaia catalog (DR1) in September 2016 promised more accurate detections of the Yarkovsky effect in a larger number of NEOs by reducing the star catalog errors by a factor of 10 or more and eliminating star catalog biases as a function of sky position (Farnocchia et al., 2015; Spoto et al., 2017). However, Gaia did not release their measured asteroid astrometry in DR1 and has some shortcomings that LCOGT does not suffer. Gaia only reaches V ≃ 19-20 (V ≃ 21.5 can be reached with the LCOGT 1.0-m network) and it never observes asteroids at opposition, removing the ability to observe asteroids at their best phase angle (Tanga and Mignard, 2012).

Gaia-DR1 (Gaia Collaboration et al., 2016) has greatly improved the quality of astrometry obtained by substantially reducing systematic catalog zonal errors (Spoto et al., 2017). The overall astrometric uncertainty is a combination of the centroiding error of the object on the CCD frame (which is unaffected by the choice of reference catalog) and systematics from the reference catalog. The switch from PPMXL (Roeser et al., 2010) to Gaia-DR1 has reduced the systematic catalog error from ≈ 300 mas to ≈ 30 mas, and the overall uncertainty (≈ 0.10″–0.18″ and ≈ 0.08″–0.21″ in the RA and Dec coordinates,

[10] https://www.minorplanetcenter.net/iau/info/OpticalObs.html.
[11] https://www.projectpluto.com/find_orb.htm.

**Table 2**
Yarkovsky signal detections for LCOGT Yarkovsky observation program. Negative $A_2$ values imply retrograde rotation (direction of rotation is opposite that of orbital motion) and inward semimajor axis drift, while positive $A_2$ values imply prograde rotation and outward drift.

| Yarkovsky Target | $A_2$ value $(AU/day)^2$ | $A_2$ uncertainty $(AU/day)^2$ | Detected SNR |
|---|---|---|---|
| (480808) 1994 XL1 | −4.8e−14 | 4.0e−15 | 12 |
| (481442) 2006 WO3 | −5.6e−14 | 1.4e−14 | 4.0 |
| (480883) 2001 YE4 | −7.0e−14 | 9.6e−16 | 73 |
| (348306) 2005 AY28 | −7.4e−14 | 1.7e−14 | 4.4 |
| (163023) 2001 XU1 | 3.9e−14 | 1.3e−14 | 3.0 |
| (192559) 1998 VO | −3.1e−14 | 8.0e−15 | 3.9 |
| 2011 EP51 | −3.2e−13 | 5.0e−14 | 6.4 |
| (364136) 2006 CJ | −2.8e−14 | 3.4e−15 | 8.2 |
| (154590) 2003 MA3 | −7.3e−14 | 1.6e−14 | 4.6 |
| (437841) 1998 HD1 | −7.0e−14 | 2.1e−14 | 3.3 |
| (326354) 2000 SJ344 | −1.7e−13 | 2.5e−14 | 6.8 |
| (499998) 2011 PT | −2.2e−13 | 3.0e−14 | 7.3 |
| 2006 TU7 | 1.7e−13 | 3.0e−14 | 5.7 |
| 2007 TF68 | −1.7e−13 | 2.8e−14 | 6.1 |
| (376879) 2001 WW1 | −5.8e−14 | 1.9e−14 | 3.1 |
| (506590) 2005 XB1 | 1.1e−13 | 1.8e−14 | 6.1 |
| (3361) 1982 HR | 2.1e−14 | 2.9e−15 | 7.2 |
| 2003 FY6 | −6.4e−14 | 1.3e−14 | 4.9 |

respectively) is now dominated by the centroiding error. With the release of DR2 in April 2018 and the availability of good reference star colors as well as the release of parallaxes and proper motions in later data releases, it would be possible to take other more subtle effects into account in the astrometric reduction. The availability of the Gaia catalog will also allow a remeasurement of past data with more accurate star catalogs. The Yarkovsky detections reported in this program made use of the Gaia-DR1 catalog only; we have not remeasured our astrometry using DR2 due to the large amount of work this would entail. It is also unlikely that the improvement in astrometric uncertainty from $\approx$ 10 mas (DR1; Gaia Collaboration et al. 2016) to $\approx$ 0.1 mas (DR2; Gaia Collaboration et al. 2018) would result in reduced uncertainty in our reported detections as the catalog uncertainty in the older DR1 release is already at least an order of magnitude smaller than our centroiding uncertainty.

## 3. Results

We observed a different set of asteroids each month as shown in Table 1. For each observed target, we assessed the astrometric uncertainties and computed an updated estimate of $A_2$ by fitting the full astrometric dataset as described in Farnocchia et al. (2013b). The results reported in this paper include all observational data available from the Minor Planet Center for each Yarkovsky candidate, including reported data available after we identified them as targets. In particular, some of our targets were additionally observed by other groups that include Tyler Linder, Robert McMillan, Dave Tholen, Marco Micheli, and their collaborators.

The LCOGT observing program helped to provide confirmation of 18 $> 3\sigma$ Yarkovsky detections (shown in Table 2) out of 36 targets measured. The remaining 18 targets yielded Yarkovsky measurements below the $3\sigma$ detection limit (shown in Table 3). Fig. 1 shows the measured $A_2$ values for all Yarkovsky candidates observed in the program. All $A_2$ measurements can also be found in the Jet Propulsion Laboratory's Small Body Database (SBDB)[12], where they were submitted upon being made.

As previously discussed in Section 2.1, Yarkovsky detections are not guaranteed for our predictions. It is possible that physical properties of the asteroids can result in lower drift rates than expected, as was the case for 50% of our targets. Further discussion of this can be found in Section 4.

**Table 3**
Observed targets for which no Yarkovsky signal was detected (i.e., $< 3\sigma$ Yarkovsky detections).

| Yarkovsky Target | $A_2$ value $(AU/day)^2$ | $A_2$ uncertainty $(AU/day)^2$ | Detected SNR |
|---|---|---|---|
| 2012 YK | −8.6e−14 | 6.6e−14 | 1.3 |
| (265482) 2005 EE | 7.2e−14 | 3.8e−14 | 1.9 |
| (494710) 2005 MO13 | −4.6e−14 | 2.8e−14 | 1.6 |
| (495829) 1995 LG | 1.8e−15 | 6.4e−15 | 0.28 |
| 2011 KE3 | −1.7e−13 | 1.1e−13 | 1.5 |
| 2003 DZ15 | −3.4e−14 | 8.0e−14 | 0.43 |
| (162183) 1999 NB5 | −5.5e−15 | 2.0e−14 | 0.28 |
| (496901) 2001 HB | −8.1e−14 | 2.9e−14 | 2.8 |
| (503941) 2003 UV11 | 6.2e−15 | 3.5e−15 | 1.8 |
| (513312) 2007 DM41 | 6.7e−14 | 3.5e−14 | 1.9 |
| (497113) 2004 EK1 | −4.5e−14 | 2.0e−14 | 2.3 |
| (506491) 2003 UW29 | 2.1e−14 | 2.4e−14 | 0.88 |
| (234145) 2000 EW70 | −1.4e−14 | 1.1e−14 | 1.3 |
| (216985) 2000 QK130 | 6.7e−14 | 2.6e−14 | 2.6 |
| (388189) 2006 DS14 | −2.6e−14 | 1.8e−14 | 1.4 |
| (267940) 2004 EM20 | −3.6e−14 | 1.9e−14 | 1.9 |
| (516435) 2004 FJ29 | −3.3e−14 | 1.7e−14 | 1.9 |
| 2010 JO33 | −6.9e−14 | 4.8e−14 | 1.4 |

We were unsuccessful at attempts to observe a handful of targets with LCOGT during the 19−month period of the program from November 2016 to May 2018 due to weather and competition on the network. These included (480820) 1998 VF32, (226514) 2003 UX34, 1995 CR, 2001 SQ263, 2000 HB24, 2012 TC4, 2006 AL4, 2016 CO246, 2010 GD35, and 2004 RQ252. Of these, 2012 TC4, 2016 CO246, and 2010 GD35 yielded $> 3\sigma$ Yarkovsky detections (SNR = 4.2, 4.0, and 3.1, respectively) from the other groups also involved in observing these targets. 1995 CR yielded a $< 3\sigma$ detection and the rest were not observed by the other groups.

## 4. Discussion

50% of our observed targets that were predicted to be the best candidates for obtaining Yarkovsky detections (see Section 2 for our target selection criteria) failed to lead to $> 3\sigma$ detections. The large fraction of predictions that did not yield a detection imply that the modeling used for the prediction and determination of the Yarkovsky effect has limitations. However, these predictions rely on typically unknown asteroid physical properties such as obliquity, rotation rate, surface thermal inertia, bulk density, and mass (Bottke et al., 2006), so it is difficult to make improvements.

As described in Section 2.1, Bennu's physical properties may result in overestimates of the magnitude of $A_2$, as our 50% detection rate would suggest. Fig. 2 shows a stacked histogram of the ratio of measured ($A_2$ + $A_2$ uncertainty) to extrapolated (from that of Bennu) $A_2$ values for all the candidates observed in the program. For all but three of the candidates, $(A_2)_{extrapolated}$>($A_2$ + $A_2$ uncertainty) with a slight gradient in the decrease of ($A_2$ + $A_2$ uncertainty) / $(A_2)_{extrapolated}$ as the SNR decreases. We find that the median overestimate of ($A_2$ + $A_2$ uncertainty) from $(A_2)_{extrapolated}$ is 2.6 for the $< 1\sigma$ detections, 1.6 for the $< 3\sigma$ detections, and 1.5 for the $> 3\sigma$ detections. However, without knowing more details about the physical properties of these individual asteroids, it will be difficult to use this information to improve predictions of additional Yarkovsky candidates in the future. It is important to be aware that $(A_2)_{extrapolated}$ is more like an upper bound than a prediction.

The discrepancy between $(A_2)_{extrapolated}$ and ($A_2$ + $A_2$ uncertainty) for most of our targets means the drift rate due to the Yarkovsky effect for these asteroids must be smaller than that of Bennu. This may point to differences in the physical properties of these asteroids compared to

[12] https://ssd.jpl.nasa.gov/sbdb.cgi.

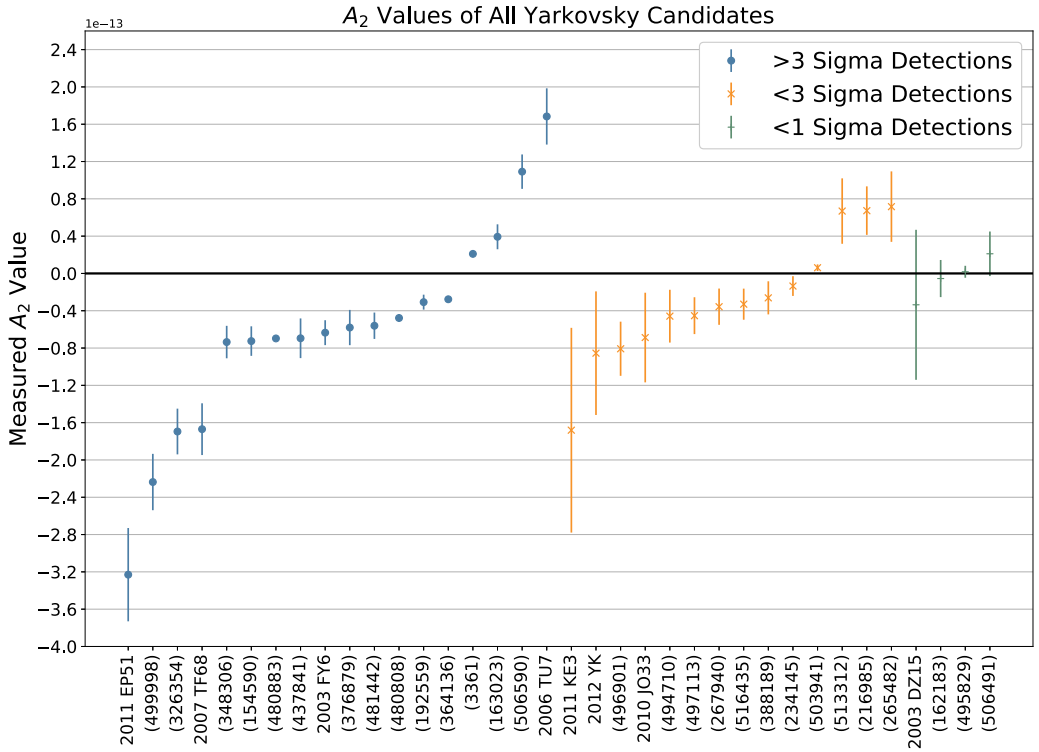


**Fig. 1.** Measured $A_2$ values for all Yarkovsky candidates observed in the program. 18 targets have $> 3\sigma$ detections (blue circle). 14 targets have $< 3\sigma$ detections (orange x) and 4 targets have $< 1\sigma$ detections (green +). Only those with $> 3\sigma$ measurements are deemed real detections.

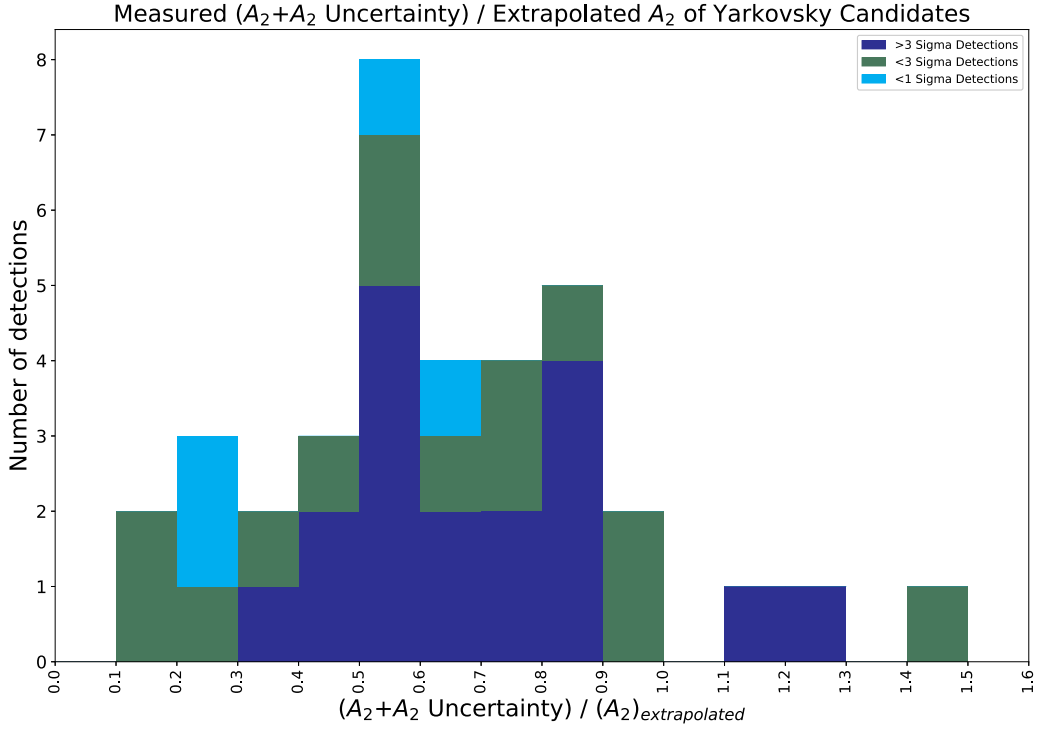


**Fig. 2.** Stacked histogram of the ratio of the measured ($A_2$ + $A_2$ uncertainty) values to the $A_2$ values extrapolated from that of Bennu using Eq. 2 for all Yarkovsky candidates observed in the program. 18 targets have $> 3\sigma$ detections (blue), 14 targets have $< 3\sigma$ detections (green), and 4 targets have $< 1\sigma$ detections (cyan). Only those with $> 3\sigma$ measurements are deemed real detections. The median overestimate of ($A_2$ + $A_2$ uncertainty) from $(A_2)_{extrapolated}$ is 2.6 for the $< 1\sigma$ detections, 1.6 for the $< 3\sigma$ detections, and 1.5 for the $> 3\sigma$ detections.

Bennu such as larger densities or mid-range obliquities (or both). However, without knowing more information about the physical properties of these asteroids, it is difficult to tell the source of the discrepancy for each asteroid.

14 out of our 18 (78%) confirmed ( $> 3\sigma$) Yarkovsky drifters are measured to be retrograde rotators (negative $A_2$ values). Farnocchia et al. (2013a) and Nugent et al. (2012) find 81% and 71%, respectively, of their measured Yarkovsky drifters to have retrograde rotation. The predominance of retrograde rotators in the NEO population is expected due to the inward drift of asteroids in the main belt into mean-motion resonances in the inner belt that raise asteroid eccentricities to the NEO region (pericenter $q < 1.3$ AU), such as the $\nu_6$ secular resonance and the 3:1 mean-motion resonance with Jupiter located in the inner main belt (Granvik et al., 2017). Bottke et al. (2002), La Spina et al. (2004), and Tardioli et al. (2017) predict the retrograde/prograde ratio from NEO feeding mechanisms to be 2:1, with which we are roughly consistent.

The observing program with LCOGT has contributed the addition of 18 asteroids to the list of Yarkovsky detections (and 18 asteroids to the list of non-detections). More discoveries, long data arcs, and higher precision data will lead to an ever-increasing list of Yarkovsky detections. These detections can aid in better-determined orbits and asteroid obliquity distributions. Yarkovsky detections can yield asteroid rotation rates and directions, which can be used to better determine the importance of resonant NEO source populations (Granvik et al., 2017). An increasing number of Yarkovsky detections can also help place constraints on physical properties of individual asteroids such as obliquity, rotation rate, surface thermal inertia, bulk density, and mass (Bottke et al., 2006). However, astrometric measurements of the Yarkovsky effect alone will not disentangle the physical properties for any given asteroid due to their coupled dependence on the Yarkovsky effect.

## Acknowledgements

This work is supported in part by NASA NEOO grant NNX14AM98G to LCOGT/Las Cumbres Observatory. Observations were performed on the LCOGT Network. D. Farnocchia conducted this research at the Jet Propulsion Laboratory, California Institute of Technology, under a contract with NASA.

## Supplementary material

Supplementary material associated with this article can be found, in the online version, at doi:10.1016/j.icarus.2018.11.032.

## References

Bertin, E., Arnouts, S., 1996. SExtractor: Software for source extraction. A&AS 117, 393–404.
Binzel, R., 2003. Planetary science: spin control for asteroids. Nature 425, 131–132.
Boroson, T., Brown, T., Hjelstrom, A., Howell, D.A., Lister, T., Pickles, A., Rosing, W., Saunders, E., Street, R., Walker, Z., 2014. Science operations for LCOGT: a global telescope network. Observatory Operations: Strategies, Processes, and Systems V. pp. 91491E.
Bottke, W.F., Vokrouhlický, D., Rubincam, D.P., Broz, M., 2002. The Effect of Yarkovsky Thermal Forces on the Dynamical Evolution of Asteroids and Meteoroids. In: Bottke, W.F., A., C., Paolicchi, P., Binzel, R.P. (Eds.), Asteroids III. University of Arizona Press, Tucson, pp. 395–408.
Bottke, W.F., Vokrouhlický, D., Rubincam, D.P., Nesvorný, D., 2006. The Yarkovsky and Yorp effects: implications for asteroid dynamics. Annu. Rev. Earth Planet. Sci. 34, 157–191.
Brown, T.M., Baliber, N., Bianco, F.B., Bowman, M., Burleson, B., Conway, P., Crellin, M., Depagne, É., De Vera, J., Dilday, B., Dragomir, D., Dubberley, M., Eastman, J.D., Elphick, M., Falarski, M., Foale, S., Ford, M., Fulton, B.J., Garza, J., Gomez, E.L., Graham, M., Greene, R., Haldeman, B., Hawkins, E., Haworth, B., Haynes, R., Hidas, M., Hjelstrom, A.E., Howell, D.A., Hygelund, J., Lister, T.A., Lobdill, R., Martinez, J., Mullins, D.S., Norbury, M., Parrent, J., Paulson, R., Petry, D.L., Pickles, A., Posner, V., Rosing, W.E., Ross, R., Sand, D.J., Saunders, E.S., Shobbrook, J., Shporer, A., Street, R.A., Thomas, D., Tsapras, Y., Tufts, J.R., Valenti, S., Vander Horst, K., Walker, Z., White, G., Willis, M., 2013. Las Cumbres Observatory Global Telescope Network. PASP 125, 1031. 1305.2437
Chesley, S.R., Farnocchia, D., Nolan, M.C., Vokrouhlický, D., Chodas, P.W., Milani, A., Spoto, F., Rozitis, B., Benner, L.A.M., Bottke, W.F., Busch, M.W., Emery, J.P., Howell, E.S., Lauretta, D.S., Margot, J.-L., Taylor, P.A., 2014. Orbit and bulk density of the OSIRIS-REx target asteroid (101955) Bennu. Icarus 235, 5–22.
Chesley, S.R., Farnocchia, D., Pravec, P., Vokrouhlický, D., 2015. Direct detections of the Yarkovsky effect: status and outlook. Proc. Int. Astron. Union 318.
Chesley, S.R., Ostro, S.J., Vokrouhlický, D., Čapek, D., Giorgini, J.D., Nolan, M.C., Margot, J.-L., Hine, A.A., Benner, L.A.M., Chamberlin, A.B., 2003. Direct detection of the Yarkovsky effect by radar ranging to asteroid 6489 Golevka. Science 302, 1739–1742.
Del Vigna, A., Faggioli, L., Milani, A., Spoto, F., Farnocchia, D., Carry, B., 2018. Detecting the Yarkovsky effect among near-Earth asteroids from astrometric data. Astron. Astrophys. 617, A61–A77.
Farnocchia, D., Chesley, S.R., 2014. Assessment of the 2880 impact threat from asteroid (29075) 1950 DA. Icarus 229, 321–327.
Farnocchia, D., Chesley, S.R., Chamberlin, A.B., Tholen, D.J., 2015. Star catalog position and proper motion corrections in asteroid astrometry. Icarus 245, 94–111.
Farnocchia, D., Chesley, S.R., Chodas, P.W., Micheli, M., Tholen, D.J., Milani, A., Elliott, G.T., Bernardi, F., 2013. Yarkovsky-driven impact risk analysis for asteroid (99942) apophis. Icarus 224, 192–200. 1301.1607
Farnocchia, D., Chesley, S.R., Tholen, D.J., Micheli, M., 2014. High precision predictions for near-Earth asteroids: the strange case of (3908) Nyx. Celest. Mech. Dyn. Astron. 119, 301–312.
Farnocchia, D., Chesley, S.R., Vokrouhlický, D., Milani, A., Spoto, F., Bottke, W.F., 2013. Near Earth asteroids with measurable Yarkovsky effect. Icarus 224, 1–13. 1212.4812
Gaia Collaboration, Brown, A.G.A., Vallenari, A., Prusti, T., de Bruijne, J.H.J., Mignard, F., Drimmel, R., Babusiaux, C., Bailer-Jones, C.A.L., Bastian, U., et al., 2016. Gaia data release 1. Summary of the astrometric, photometric, and survey properties. A&A 595, A2. 1609.04172
Gaia Collaboration, Lindegren, L., Hernandez, J., Bombrun, A., Klioner, S., Bastian, U., Ramos-Lerate, M., et al., 2018. Gaia data release 2. the astrometric solution. A&A. Accepted
Giorgini, J.D., Benner, L.A., Ostro, S.J., Nolan, M.C., Busch, M.W., 2008. Predicting the Earth encounters of (99942) Apophis. Icarus 193, 1–19.
Giorgini, J.D., Ostro, S.J., Benner, L.A., Chodas, P.W., Chesley, S.R., Hudson, R.S., Nolan, M.C., Klemola, A.R., Standish, E.M., Jurgens, R.F., Rose, R., Chamberlin, A.B., Yeomans, D.K., Margot, J.-L., 2002. Asteroid 1950 DA's encounter with Earth in 2880: physical limits of Collision probability prediction. Science 296, 132–136.
Granvik, M., Morbidelli, A., Vokrouhlický, D., Bottke, W.F., Nesvorný, D., Jedicke, R., 2017. Escape of asteroids from the main belt. Astron. Astrophys. 598, A52–A6410.1051/0004–6361/201629252.
Greenberg, A. H., Margot, J.-L., Verma, A. K., Taylor, P. A., Hodge, S. E., 2017. Yarkovsky Drift Detections for 159 near-Earth Asteroids1708.05513.
La Spina, A., Paolicchi, P., Kryszczyńska, A., Pravec, P., 2004. Retrograde spins of near-Earth asteroids from the Yarkovsky effect. Nature 428, 400–401.
Lang, D., Hogg, D.W., Mierle, K., Blanton, M., Roweis, S., 2010. Astrometry.net: blind astrometric calibration of arbitrary astronomical images. AJ 139, 1782–1800. 0910.2233
Lister, T., Gomez, E., Greenstreet, S., 2015. The LCOGT NEO follow-up network. IAU Gen. Assem. 22, 2258398.
McCully, C., Volgenau, N.H., Harbeck, D.-R., Lister, T.A., Saunders, E.S., Turner, M.L., Siverd, R.J., Bowman, M., 2018. Real-time processing of the imaging data from the network of Las Cumbres Observatory telescopes using banzai. Observatory Operations: Strategies, Processes, and Systems VII,. pp. 107070K.
Mommert, M., Hora, J.L., Farnocchia, D., Chesley, S.R., Vokrouhlický, D., Trilling, D.E., Mueller, M., Harris, A.W., Smith, H.A., Fazio, G.G., 2014. Constraining the physical properties of near-Earth object 2009 BD. ApJ 786, 148–166.
Nugent, C.R., Margot, J.-L., Chesley, S.R., Vokrouhlický, D., 2012. Detection of semimajor axis drifts in 54 near-Earth asteroids: new measurements of the Yarkovsky effect. AJ 144, 60–72.
Roeser, S., Demleitner, M., Schilbach, E., 2010. The PPMXL catalog of positions and proper motions on the ICRS. Combining USNO-B1.0 and the Two Micron All Sky Survey (2MASS). AJ 139, 2440–2447. 1003.5852
Saunders, E.S., Lampoudi, S., Lister, T.A., Norbury, M., Walker, Z., 2014. Novel scheduling approaches in the era of multi-telescope networks. Observatory Operations: Strategies, Processes, and Systems V. pp. 91490E..
Skrutskie, M.F., Cutri, R.M., Stiening, R., Weinberg, M.D., Schneider, S., Carpenter, J.M., Beichman, C., Capps, R., Chester, T., Elias, J., Huchra, J., Liebert, J., Lonsdale, C., Monet, D.G., Price, S., Seitzer, P., Jarrett, T., Kirkpatrick, J.D., Gizis, J.E., Howard, E., Evans, T., Fowler, J., Fullmer, L., Hurt, R., Light, R., Kopan, E.L., Marsh, K.A., McCallon, H.L., Tam, R., Van Dyk, S., Wheelock, S., 2006. The Two Micron All Sky Survey (2MASS). AJ 131, 1163–1183.
Spoto, F., Milani, A., Farnocchia, D., Chesley, S.R., Micheli, M., Valsecchi, G.B., Perna, D., Hainaut, O., 2014. Nongravitational perturbations and virtual impactors: the case of asteroid (410777) 2009 FD. A&A 572, A100.
Spoto, F., Tanga, P., Bouquillon, S., Desmars, J., Hestroffer, D., Mignard, F., Altmann, M., Herald, D., Marchant, J., Barache, C., Carlucci, T., Lister, T., Taris, F., 2017. Ground-based astrometry calibrated by Gaia DR1: new perspectives in asteroid orbit determination. A&A 607, A21.
Tanga, P., Mignard, F., 2012. The Solar System as seen by Gaia: the asteroids and their accuracy budget. Planet. Space Sci. 73, 5–9.
Tardioli, C., Farnocchia, D., Rozitis, B., Cotto-Figueroa, D., Chesley, S.R., Statler, T.S., Vasile, M., 2017. Constraints on the near-Earth asteroid obliquity distribution from the Yarkovsky effect. A&A 608, A61–A69.
Tonry, J.L., Stubbs, C.W., Lykke, K.R., Doherty, P., Shivvers, I.S., Burgett, W.S., Chambers, K.C., Hodapp, K.W., Kaiser, N., Kudritzki, R.-P., Magnier, E.A., Morgan,

J.S., Price, P.A., Wainscoat, R.J., 2012. The Pan-Starrs1 photometric system. ApJ 750 (2), 99.
Vokrouhlický, D., Bottke, W.F., Chesley, S.R., Scheeres, D.J., Statler, T.S., 2015. The Yarkovsky and YORP effects. In: Michel, P., DeMeo, F.E., Bottke, W.F. (Eds.), Asteroids IV. University of Arizona Press, Tucson, pp. 509–531. 4
Vokrouhlický, D., Chesley, S.R., Matson, R.D., 2008. Orbital Identification for Asteroid 152563 (1992 Bf) through the Yarkovsky effect. AJ 135, 2336–2340.
Vokrouhlický, D., Farnocchia, D., Čapek, D., Chesley, S.R., Pravec, P., Scheirich, P., Müller, T.G., 2015. The Yarkovsky effect for 99942 Apophis. Icarus 252, 277–283.
Volgenau, N., Boroson, T., 2016. Two years of LCOGT operations: the challenges of a global observatory. Observatory Operations: Strategies, Processes, and Systems VI. pp. 99101C.